PCCP

Accepted Manuscript

A Detailed Study on Working Mechanism of Heteropoly Acid Modified TiO$_2$ Photoanode for Efficient Dye-Sensitized Solar Cells

Yanxia Jiang,[a] Yulin Yang,[*a] Liangsheng Qiang,[a] Ruiqing Fan,[*a] Liang Li,[a] Tengling Ye,[a] Yong, Na,[a] Yan Shi,[a] Tianzhu, Luan[b]

[a]*Department of Chemistry, Harbin Institute of Technology, Harbin, 150001, P. R. China.*

[b]*The First Affiliated Hospital of Harbin Medical University, Harbin, 150001, P. R. China.*

To whom the correspondence should be addressed.

Prof. Yulin Yang and Prof. Ruiqing Fan

Department of Chemistry

Harbin Institute of Technology, Harbin 150001, P. R. China

Fax: +86-451-86418270

E-mail: ylyang@hit.edu.cn and fanruiqing@hit.edu.cn

A novel heteropolyacid (HPA) $K_6SiW_{11}O_{39}Ni(H_2O) \cdot xH_2O$ ($SiW_{11}Ni$) modified TiO_2 has been successfully synthesized and introduced into the photoanode of dye-sensitized solar cells (DSSCs). The performance of the cell with the HPA-modified photoanode ($SiW_{11}Ni/TiO_2$), mixed with P25 powder in the ratio of 2:8 is better than the cell with a pristine P25 photoanode. An increase of 31% in the photocurrent and 22% improvement in the conversion efficiency are obtained. The effect of the heteropolyacid was well studied by UV–vis spectroscopy, spectro-electrochemical spectroscopy, dark current, intensity-modulated photocurrent spectroscopy and intensity-modulated photovoltage spectroscopy, open-circuit voltage decay and electrochemical impedance spectra. The results show that the interfacial layer modified by $SiW_{11}Ni$ can enhance the electrons injection, transport, and then retard the recombination of electrons, which results in a longer electrons lifetime. What's more, the introduction of $SiW_{11}Ni$ can simultaneously broaden the absorption to the visible region, eventually leading to an efficient increase in energy conversion efficiency.

1   **Introduction**

2   The dye-sensitized solar cells (DSSCs) developed by Grätzel have been widely

3   studied by researchers due to their low cost, high efficiency and easy fabrication.[1-4]

4   The typical device structure of DSSCs is composed of a dye-sensitized semiconductor

5   photoanode, an electrolyte with a redox couple, and a counter electrode.[5]

6   Semiconductor photoanode is one of the key factors that affect the final device

7   performance because it relates directly to the light absorption and electrons transport

8   in DSSCs. TiO_2 is the most common photoanodes used in DSSCs. To develop more

9   efficient TiO_2 photoanodes, many studies have been done and they mainly

10 concentrated on enhancing the photoabsorption, tuning the energy level, the charge

11 transport and retarding the charge recombination.[6-12]

12   Polyoxometalates (POMs), a class of inorganic anionic clusters, have been

13 widely applied in medicine, magnetism, nonlinear optics, and catalysis because of

14 their versatile properties.[13-19] Recently, POMs have been introduced into DSSCs to

15 modify photoanodes. Chen et al. developed a $H_3PW_{12}O_{40}$-based TiO_2 photoanode and

16 they found that $H_3PW_{12}O_{40}$-based TiO_2 photoanode can accelerate electrons transfer

17 and retard recombination, eventually leading to a 19% increase in photocurrent.[20] Xu

18 et al. prepared multilayer film photoanodes consisting of TiO_2 nanoparticles, gold

19 nanoparticles (Au) and Dawson-type polyoxometalate $K_6P_2W_{18}O_{62}$ by the

20 layer-by-layer self-assembly method, and poly(styrenesulfonate) (PSS) was used as a

21 film forming auxiliary material. They found that $K_6P_2W_{18}O_{62}$ could also retard charge

22 pair recombination and enhanced the photovoltaic performance of DSSC with an

23 efficiency of 0.014%.[21] These pioneering studies indicate that POMs are promising

24 candidates to modify the photoanode in DSSCs and to enhance the cell performance.

25   In this work, we synthesized a novel kind of $SiW_{11}Ni$ modified TiO_2

26 semiconductor ($SiW_{11}Ni/TiO_2$). By mixing $SiW_{11}Ni/TiO_2$ with P25 in different mass

27 ratio (2:8, 3:7, 4:6, 1:1) and applying them as photoanodes in DSSCs, the

28 performance of the cells was enhanced dramatically compared to the pristine P25 cell.

29 A 31% and 22% of improvement in the photocurrent and efficiency was obtained for

1   the DSSC using $SiW_{11}Ni/TiO_2$:P25=2:8 as the photoanode. Comparing to the

2   pioneering studies, $SiW_{11}Ni$ modified TiO_2 as a photoanode has a better performance

3   on the absorption of visible light and power conversion efficiency. We have studied

4   the working mechanism for $SiW_{11}Ni/TiO_2$ in DSSCs in detail. The light absorption,

5   electrons injection, electrons transport, charge recombination and the physical

6   processes of enhancing the efficiency of electron transfer behavior of the $SiW_{11}Ni$

7   modified TiO_2 were well studied by UV–vis spectroscopy, spectro-electrochemical

8   spectroscopy, dark current, intensity-modulated photocurrent spectroscopy (IMPS)

9   and intensity-modulated photovoltage spectroscopy (IMVS), open-circuit voltage

10   decay (OCVD), and electrochemical impedance spectra (EIS) respectively. A working

11   mechanism of $SiW_{11}Ni/TiO_2$-P25 photoanode for efficient DSSCs has been proposed.

12   ## Experimental section

13   **Synthesis of $SiW_{11}Ni$ and $SiW_{11}Ni/TiO_2$**

14   $SiW_{11}Ni$ was synthesized using similar method as discussed in the literature.[22]

15   According to FT-IR spectrum shown in (Fig. S1a, ESI), the characteristic stretching

16   vibrations for $SiW_{11}Ni$ were observed at 953 cm^{-1} (W-O$_d$), 908 cm^{-1} (Si-O$_a$), 790 cm^{-1}

17   (W-O$_b$-W) and 704 cm^{-1} (W-O$_c$-W), respectively.[23] The same peak at 527 cm^{-1}

18   confirmed the Keggin structure of $SiW_{11}Ni$ as reported in the literature.[24] Fig. S1b

19   (ESI) shows the TG curve of $SiW_{11}Ni$ and a high thermal stability can be observed.

20   $\quad$ TiO_2 was modified with $SiW_{11}Ni$ through a hydrothermal method. 0.5 mL HNO_3

21   was diluted into 60mL deionized water in flask. 10mL titanium tetraisopropoxide was

22   slowly added with stirred vigorously. Then 0.1 g $SiW_{11}Ni$ was added and a flaky

23   white precipitate could be obtained. This solution with vigorous stirring was kept

24   around 98 ℃ for 3 hours, the white precipitate would be re-dissolved and produce an

25   opaque solution. The opaque solution was transferred into a 25 mL Teflon-lined

26   stainless steel autoclave and maintained in an electric oven at 200 °C for 24 hours.

27   After natural cooling to room temperature, it was centrifuged and washed

28   thoroughly with deionized water and absolute ethanol. After dried at 100 °C in

29   vacuum, the precipitate was calcined at 450 °C for 30 minutes and then cooled to

1   room temperature. Finally $SiW_{11}Ni$ modified TiO_2 powders were obtained. Fig. S2a

2   (ESI) shows the high resolution XPS spectra of Ti 2p. Ti 2p3/2 and Ti 2p1/2 are

3   situated at 458.9 and 464.7 eV for pristine TiO_2. After modifying, both of them shifted

4   toward lower binding energy of about 0.2 eV. This slight change of Ti 2p peaks and

5   5.8 eV between Ti 2p3/2 and Ti 2p1/2 indicates they are Ti^{4+}. Similar shift was

6   previously attributed to the change of the local chemical environment of Ti ions

7   influenced by $SiW_{11}Ni$ incorporation and to the formation of Ti···O bonds on the

8   surface of TiO_2. So, Ti 2p will shift to lower binding energy, and the peaks become

9   slightly broader.[25] Fig. S2b (ESI) displays the O 1s spectra comparison $SiW_{11}Ni/TiO_2$

10   and pristine TiO_2 samples. The O 1s region of the pristine TiO_2 is located at 530.2 eV,

11   while the peak of $SiW_{11}Ni/TiO_2$ centered at 530.0 eV, further confirming the presence

12   of Ti···O weak interaction. The slight shift of these peaks can be attributed to the

13   hydrothermal conditions, which can reduce the number of defects and impurities in

14   TiO_2.

15   **Preparation of Photoanodes and Cell Assembly Photoanode**

16   All photoanodes were fabricated using a screen printing method. There are two kinds

17   of samples for photoanodes: photoanode $SiW_{11}Ni/TiO_2$ blended with TiO_2

18   nanoparticles (commercial Degussa P25 nanoparticles, which consists of about 20 %

19   rutile and 80 % anatase and a particle size of about 25 nm) in a weight ratio of 2:8 and

20   pristine TiO_2 paste without modified for comparison. Ethyl cellulose and α-terpineol

21   were used as a binder to disperse the mixed powers while ethanol was used as

22   dispersant. Then the ethanol was removed using rotary evaporation. The resulting

23   slurry was screened-printed onto F-doped SnO_2-coated conductive glass plate (FTO,

24   90% transmittance in the visible region, 15 $\Omega\ cm^{-2}$) and sintered at 450 °C for 15 min.

25   The photoanode film with thickness of 8 μm and active area 0.16 cm^2 was covered on

26   the FTO substrate by using the screen printing method to create 4 mm × 4 mm

27   electrodes. Fig. S3 (ESI) shows the images of pristine TiO_2 and $SiW_{11}Ni/TiO_2$. After

28   modifying with $SiW_{11}Ni$, we can see some big blocks among TiO_2 particles.

29   The $SiW_{11}Ni/TiO_2$-P25 and pristine TiO_2 (P25) photoanodes were then immersed

30   in absolute ethanol solution containing 0.3 mM N719 (Solaronix SA, Switzerland)

31   and kept at room temperature for 24 hours. The sandwich-type solar cell was

1 assembled by placing a platinum-coated conductive glass as counter electrode on the

2 N719 dye-sensitized photo-anode, a drop of liquid electrolyte with 0.5 M LiI, 0.05 M

3 I_2, 0.1 M TBP (4-tert-butylpyridine) was added to fill the void between two electrodes

4 and clipping together as open cells for measurement.

5 **Characterization**

6 Scanning electrons microscope (SEM) micrograph was analyzed by FEI Company

7 Helios Nanolab 600i focused ion electrons double beam SEM. Fourier transform

8 (FT)-IR spectra were measured on a Perkin-Elmer Spectrum 100 FT-IR Spectrometer

9 with samples prepared as KBr pellet. Thermogravimetric (TG) analyses were

10 performed on Perkin-Elmer STA 6000 Simultaneous Thermal Analyzer with a heating

11 rate of 10 °C/min in flowing nitrogen atmosphere. UV-vis spectra were recorded by a

12 UV-2250 spectrophotometer (Shimadzu, Japan). A custom jacketed three electrodes

13 electrochemical cell was incorporated into an Agilent Technologies Cary 60 UV-vis

14 spectrophotometer such that the mesoporous TiO_2 film was positioned normal to the

15 optical path. The photocurrent-photovoltage ($J-V$) curves were recorded by CHI660D

16 electrochemical analyzer. The light intensity of AM1.5 global sunlight from a filtered

17 500 W xenon lamp (CHF-XM500, Changtuo, China with an AM1.5 global filter from

18 Newport) was calibrated by a standard Si solar cell (calibrated at National Institute of

19 Metrology, P. R. China). EIS and OCVD were recorded by CHI660D Electrochemical

20 Analyzer (Chenhua, China) and the applied forward bias was generally −0.8 V while

21 IMPS-IMVS were obtained by applied voltage under an illumination with different

22 light intensities from 30 to 150 $W \cdot m^{-2}$. A 300 W Xe lamp was used for incident

23 photon-to-current quantum conversion efficiency (IPCE) measurements, a

24 monochromator (Newport 74125) with sorting filters focused on a spot with

25 additional optics. The current response of the devices was recorded in 10 nm

26 increments using a power meter (Newport 2936−C). The measured currents were

27 referenced to a calibrated Silicon detector (Newport 71675).

28 **Results and discussion**

29 We mixed the new composite material $SiW_{11}Ni/TiO_2$ with P25 in different mass ratio

1 and applied them as photoanode in DSSC and bare P25 based DSSC was also

2 fabricated for comparison. Photovoltaic parameters of a series of DSSCs based on

3 $SiW_{11}Ni/TiO_2$-P25 are listed in Table 1. As the wt % of $SiW_{11}Ni$ increased, η rises

4 first and then descends. When the blending ratio is 2:8, the cell gives the best

5 performance. This may attribute to the higher $SiW_{11}Ni/TiO_2$ contents brought about

6 more grain boundaries for more recombination within DSSCs and result in the poor

7 performance. Fig. 1 shows the optimized current density-voltage (*J-V)* curves of the

8 P25- and $SiW_{11}Ni/TiO_2$-P25-based DSSCs. The DSSC based on $SiW_{11}Ni/TiO_2$-P25

9 photoanode gives a short circuit current density (J_{sc}) of 17.38 mA cm^{-2}, an open

10 circuit voltage (V_{oc}) of 0.73 V and a fill factor of (*FF*) 0.61, resulting in a power

11 conversion efficiency (η) of 7.82%. Comparing with that of the DSSC using bare P25

12 as the photoanode, a 31% and 22% increase in J_{sc} and η was obtained. The

13 performance of P25 is analogous to the references.[26−29]

14 **Table 1** Photovoltaic parameters of a series of DSSCs based on $SiW_{11}Ni/TiO_2$-P25,

15 measured under 100 mW cm^{-2} (AM1.5G) illuminations. The active areas were 0.16

16 cm^2 for all of the cells (with the mask area 0.25 cm^2).

$SiW_{11}Ni/TiO_2$-P25	J_{sc}/mA cm^{-2}	V_{oc}/mV	*FF*	η%
P25	13.28	0.76	0.64	6.42
1:9	15.49	0.75	0.59	6.93
2:8	17.38	0.73	0.61	7.82
3:7	14.22	0.70	0.57	5.66
4:6	13.54	0.69	0.55	5.11
5:5	12.61	0.65	0.57	4.67
6:4	12.28	0.65	0.57	4.51
7:3	11.98	0.64	0.56	4.29
8:2	11.21	0.64	0.56	4.02
9:1	10.34	0.64	0.55	3.64
10:0	10.01	0.63	0.55	3.47

1
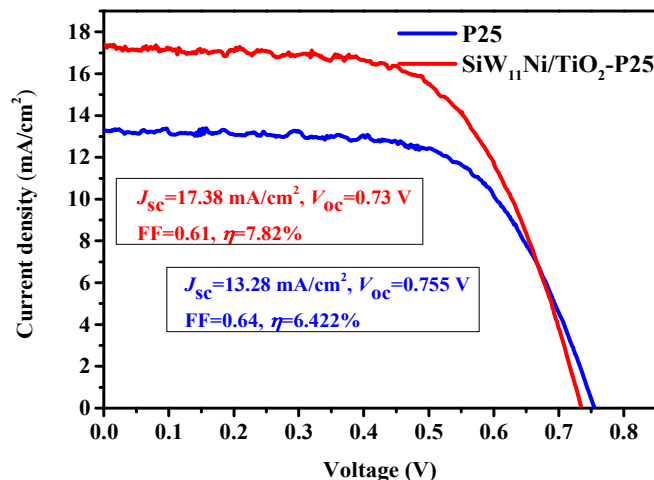
Fig. 1 The current density versus voltage curves of dye-sensitized solar cells based on the P25 and

SiW$_{11}$Ni/TiO$_2$-P25 photoanodes under 100 mW cm^{-2} (AM1.5G) illuminations.

4
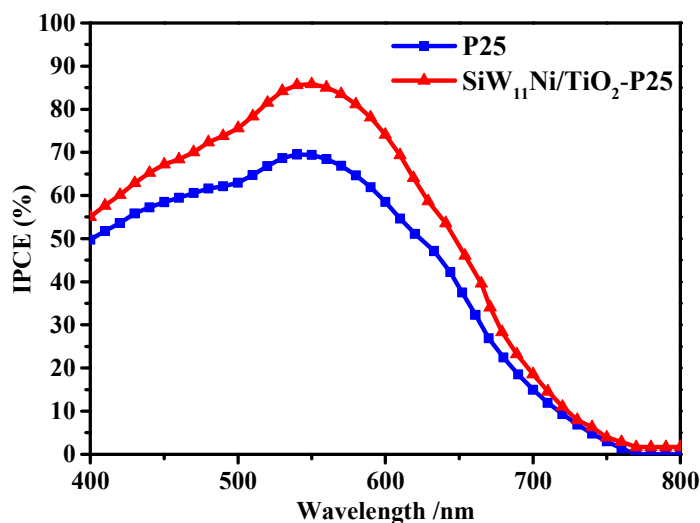
Fig. 2 IPCE spectra of the DSSCs based on P25 and SiW$_{11}$Ni/TiO$_2$-P25 photoanodes.

The corresponding IPCE spectra of the DSSCs were also measured and shown in

Fig. 2, the photoanode DSSC based on SiW$_{11}$Ni/TiO$_2$-P25 exhibits a significant effect

on absorbed photon-to-collected electron efficiency. The improvement of the charge

collection yield in the IPCE spectra were in good agreement with the measured

photocurrent density. To explore the reason of the enhancement, we studied on the

working mechanism of SiW$_{11}$Ni modified TiO$_2$ in detail.

Fig. 3 shows the UV-visible absorption spectra and the band gap (the inset graph)

of TiO$_2$ and SiW$_{11}$Ni/TiO$_2$. For both pristine SiW$_{11}$Ni and SiW$_{11}$Ni/TiO$_2$, an

absorption in the visible region is observed. It is well known that TiO$_2$ only absorb

1   UV light (λ < 387 nm) without any absorption in visible and infrared regions. After

2   the modification with $SiW_{11}Ni$, the absorption of TiO_2 in the visible region changed

3   obviously from 365 nm to 525 nm, which effectively compensates the weak

4   absorption of titania in the visible region. More importantly, N719 has weak

5   absorption in the range of 400 nm~450 nm and this compensation effect is conducive

6   to improve the utilization efficiency of light as shown in Fig. S4 (ESI). The band gap

7   of the $SiW_{11}Ni/TiO_2$ is found to be 2.92 eV which is lower than the band gap of the

8   TiO_2 (3.14 eV). According to the Tauc plot equation, the direct band gap energies of

9   samples are calculated using the point of intersection of the tangents to the plots of

10   $(\alpha hv)^2$ vs (hv).[30] In addition, the reduction of the band gap energy of $SiW_{11}Ni/TiO_2$

11   compared to the pristine TiO_2 indicates that an obvious red shift on the absorbance

12   toward the visible region and increasing energy difference from the LUMO of N719

13   to the CB of TiO_2, and then increase the driving force of the electrons injection.
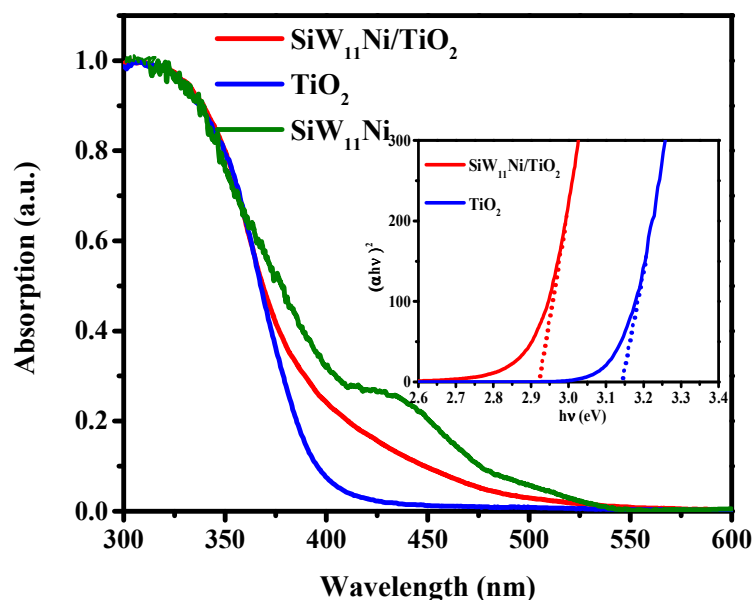
14

15   **Fig. 3** UV-visible absorption spectra of TiO_2, $SiW_{11}Ni$ and $SiW_{11}Ni/TiO_2$ and Tauc polt

16   representing band gap energy of TiO_2 and $SiW_{11}Ni/TiO_2$ (inset graph).

17   To make clear the contribution of $SiW_{11}Ni/TiO_2$ in the electrons injection and

18   transport, spectro-electrochemistry spectroscopy and dark current were studied. The

19   chemical capacitance of the TiO_2 and $SiW_{11}Ni/TiO_2$ photoanode films as a function of

20   applied potential was measured and shown in Fig. 5a. The chemical capacitance of

1   SiW$_{11}$Ni/TiO$_2$ film leftward shifts compared with that of the pristine TiO$_2$ film, which

2   is because of the band edge of SiW$_{11}$Ni/TiO$_2$ decrease downward the I$_3^-$/I$^-$ potential.

3   From Fig. 5a, we can deduce the flat band potential (V_{fb}) which is a very important

4   parameter in spectro-electrochemistry and it can directly reflect the location of the

5   energetic position of the valence band and conduction band edge of a given

6   semiconductor material. Michael Grätzel proposed that the main contribution to the

7   optical absorption at 780 nm comes from interband transitions or from free carrier

8   absorption, therefore the absorbance is proportional to the density of electrons in the

9   conduction band.[31] The V_{fb} of TiO$_2$ and SiW$_{11}$Ni/TiO$_2$ was shown in Fig. 5b. We can

10   see that the absorbance of TiO$_2$ and SiW$_{11}$Ni/TiO$_2$ transparent films at 780 nm with

11   the applied potential. By introducing SiW$_{11}$Ni into the photoanode, the V_{fb} of TiO$_2$

12   (around -0.6 V) positively shifts to -0.4 V, which indicates the Fermi level of

13   SiW$_{11}$Ni/TiO$_2$ is lower than pristine TiO$_2$. The shift of conduction band edge will be

14   accompanied by an equal displacement of quasi-Fermi level relative to the I$_3^-$/I$^-$ Fermi

15   level. If the band edge shifts positively, the electrons quasi-Fermi level also shifts

16   toward the positive direction.[32,33] The lower Fermi level increases the energy gap

17   between the LUMO of the dye and the conduction band of TiO$_2$, which results in an

18   enhanced injection driving force of electrons and then improves the photogenerated

19   electrons injection efficiency from the LUMO of dye to the conduction band of TiO$_2$.

20   This result will benefit for charge transfer.[34] At the same time, the recombination

21   between injected electrons, dye cations and iodide ions is reduced.[35-37] In addition, the

22   decrease of the Fermi level of SiW$_{11}$Ni/TiO$_2$ results in the decrease of V_{oc}. It is

23   because V_{oc} is related to the difference between the Fermi level of the photoanode and

24   the redox potential of the electrolyte.[38,39] The schematic energy level diagram for the

25   electrode interface is presented in Scheme S1 (ESI).
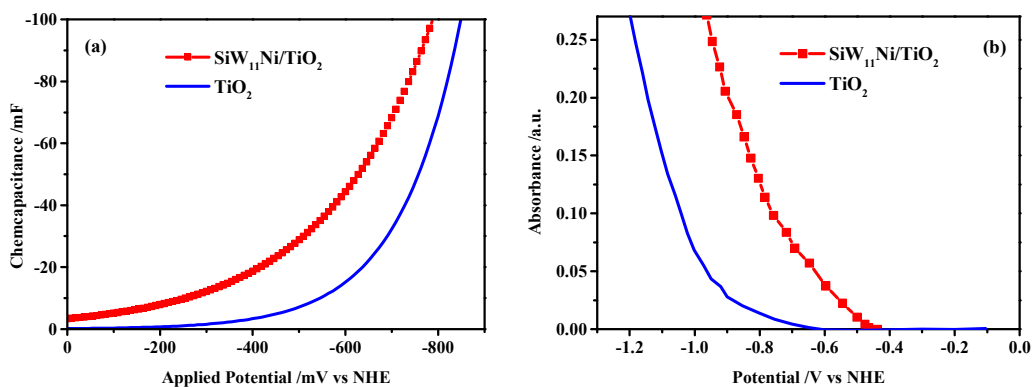
1

2   **Fig. 5** (a) Chemical capacitance of the TiO_2 and $SiW_{11}Ni/TiO_2$ photoanode film while the films

3   were immersed into 0.1 M $LiClO_4$ as a function of applied potential; (b) Optical absorbance at 780

4   nm of the TiO_2 and $SiW_{11}Ni/TiO_2$ photoanode film.

5   The electrons transfer of $SiW_{11}Ni/TiO_2$ was studied by the dark current vs

6   voltage. As shown in Fig. 6a, the onset of the dark current of the bare DSSC occurred

7   at 0.3V, whereas for the $SiW_{11}Ni/TiO_2$ based DSSC, the onset of the dark current was

8   suppressed. The reduction of the dark current demonstrates that the $SiW_{11}Ni$ based

9   photoanode successfully reduced the recombination reaction of the electrons.

10   Therefore, the dark current density in the DSSCs with $SiW_{11}Ni$ was obviously

11   suppressed, which enhanced the η values of the DSSCs.[40] The result is also supported

12   by the outcome of IMPS-IMVS shown in the following.
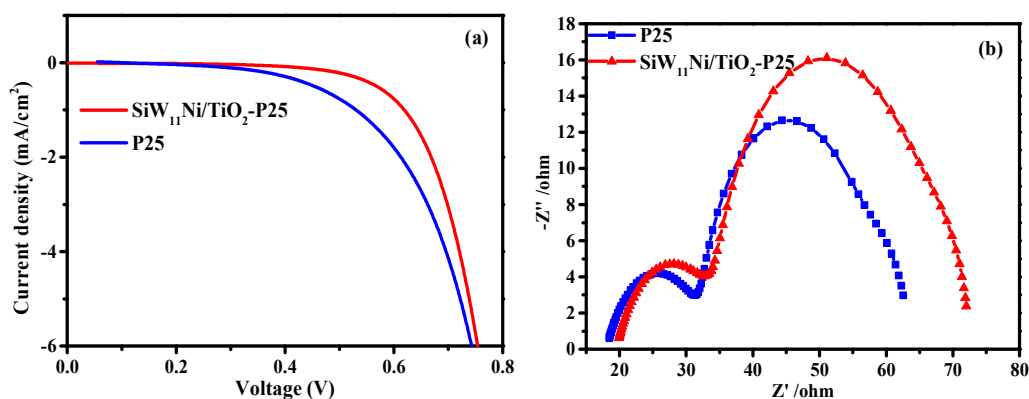
13

14   **Fig. 6** (a) The dark current density versus voltage curves and (b) Nyquist plots of electrochemical

15   impedance spectra of devices P25 and $SiW_{11}Ni/TiO_2$-P25 in dark.

16   Electrochemical impedance spectroscopy was used to study the electron transport

17   behavior and the internal resistances of the DSSCs.[41] Fig. 6b is the EIS measurements

18   that we carried out in the dark to further determine the effect of $SiW_{11}Ni$ modified

11

1   TiO$_2$ about electron recombination progress. In the dark, there were no electrons

2   injected from dye sensitizer into TiO$_2$ network, electrons were just transported

3   through the TiO$_2$ nanoparticles and reacted with the redox electrolyte (I$_3^-$). Fig. S5

4   (ESI) is the equivalent circuit obtained by using transmission line model:

5    $R_s(C_1(R_1O))(R_2Q_2)$. The series resistance (R_s) can account for the resistance of the

6   FTO glass substrate, the contact resistance of the cell and the resistance of the external

7   circuits. The semicircle in high frequency corresponds to R_2, which represents the

8   charge transfer resistance at the counter electrode/electrolyte interface; the second

9   semicircle (R_1) in the intermediate frequency region reflects the electron transport

10   resistance in the photoanode/dye/electrolyte interface related to the charge

11   transport/recombination. The corresponding parameters obtained by the equivalent

12   circuit were listed in Table 2. The two values of R_2 are similar because of the identical

13   Pt counter, and the R_1 values of P25 and SiW$_{11}$Ni/TiO$_2$-P25 are 11.08 and 28.77 ohm

14   respectively, which indicates the SiW$_{11}$Ni/TiO$_2$ photoanode based DSSC is better at

15   retarding the recombination progress than the pristine TiO$_2$ between the injected

16   electron and the redox electrolyte. The EIS result is in good agreement with the dark

17   current discussed above.

18   **Table 2** Parameters obtained by the equivalent circuit.

DSSC	R_s/Ω cm^2	R_1/Ω cm^2	R_2/Ω cm^2
P25	18.92	11.08	13.97
SiW$_{11}$Ni/TiO$_2$-P25	19.36	28.77	13.82

19   In DSSCs, the electrons recombination time (τ_n) and the electrons transport time

20   (τ_d) are very important factors for the performance of DSSCs. They are the

21   consequence of the competition between the recombination and transport of electrons

22   across the photoanode. τ_n and τ_d are calculated by IMVS and IMPS measurements

23   through eq (1) and (2) respectively:[42,43]

24
$$\tau_n = \frac{1}{2\pi f_n} \quad (1)$$

25
$$\tau_d = \frac{1}{2\pi f_d} \quad (2)$$

1   where f_n and f_d are the characteristic frequency minima of the IMVS and IMPS

2   imaginary components, respectively. The τ_n and τ_d of P25 and $SiW_{11}Ni/TiO_2$-P25 as a

3   function of the incident light intensity are shown in Fig. 7. Fig. 7a and 7b show the τ_n

4   and τ_d of the DSSCs based on two different photoanodes noted above. τ_n of

5   $SiW_{11}Ni/TiO_2$-P25 is higher than that of P25 while τ_d of $SiW_{11}Ni/TiO_2$-P25 is lower

6   than that of P25. It is because the excellent electrons injection and good electrons

7   transport of the $SiW_{11}Ni/TiO_2$-P25 photoanode, which suppresses the excited

8   electrons to react with iodine in the interfacial region between the electrolyte and the

9   photoanode. The above results strongly demonstrate that the prepared

10   $SiW_{11}Ni/TiO_2$-P25 is a promising photoanode candidate for the DSSCs.
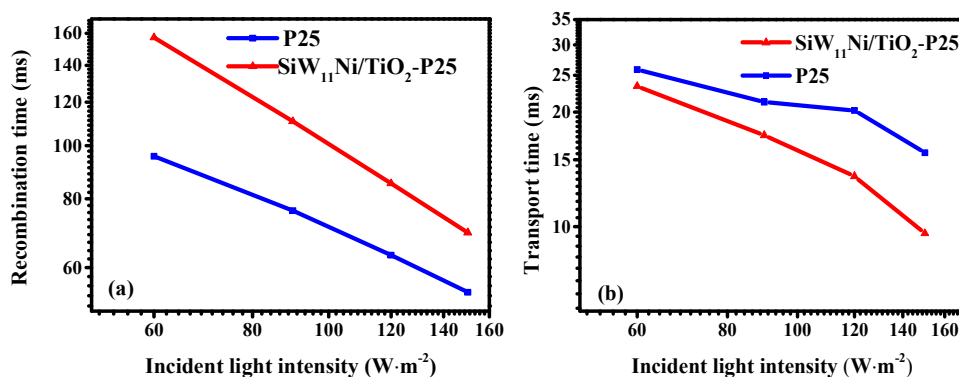
11

12   **Fig. 7** The IMVS response (a) and IMPS response (b).

13   The electrons recombining with the electrolytes can be further revealed by the

14   open-circuit voltage decay (OCVD) technique which monitors the decay of V_{oc} after

15   turning off the illumination in a setting time.[44,45] Fig. 8a shows the OCVD curves of

16   the DSSCs with the pristine P25 and $SiW_{11}Ni/TiO_2$-P25 photoanodes. It can be seen

17   that the electrons lifetime in the DSSCs with $SiW_{11}Ni/TiO_2$-P25 photoanode was

18   longer than that of pristine P25, which indicates that its rate of decay is much slower.

19   The recombination rate between electrons and the oxide electrolyte has been

20   restrained effectively, finally resulting in the much longer electrons lifetime. Fig. 8b

21   shows the electrons lifetime derived from equation (3) as a function of V_{oc}.

22
$$\tau_n = -\frac{Tk_B}{e}\left(\frac{dV_{oc}}{dt}\right)^{-1} \tag{3}$$

1   The electrons lifetime of pristine TiO_2 photoanode was shorter than that of the

2   modified one. The results were consistent with the ones we concluded from IMVS

3   and IMPS.
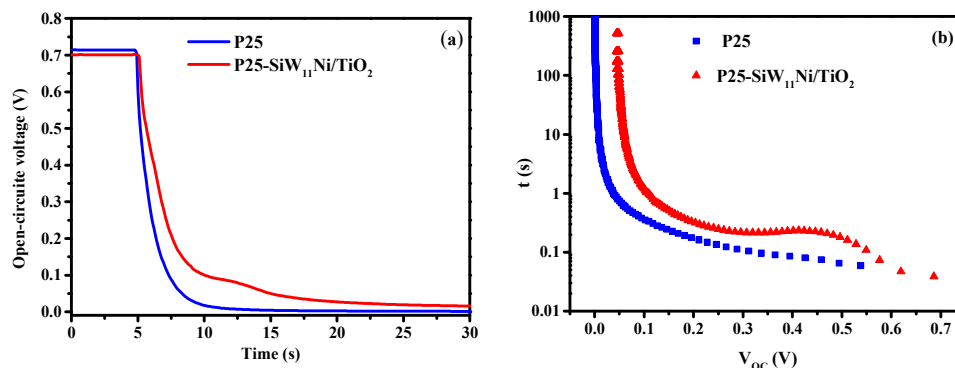
4

5   **Fig. 8** (a) The OCVD curves of the DSSCs with P25 and $SiW_{11}Ni/TiO_2$-P25 photoanodes and (b)

6   the electrons lifetime derived from equation (3) as a function of V_{oc}.

7   Based on the above analyzation, the considerable improvement in J_{sc} and η can

8   be attributed to the following reasons: (1) for the modified TiO_2, the flat band (V_{fb})

9   (about -0.6 V) shifts positively to -0.4 V. This result increases the driving force for

10   electrons injection, improving the electrons injection efficiency from the LUMO of

11   N719 to the conduction band of TiO_2. The modified $SiW_{11}Ni$ on TiO_2 also improves

12   the electrons transport. The improved electrons injection and transport for the new

13   photoanode restrains the electrons recombining between the oxide electrolyte and dye

14   cations effectively and prolongs the lifetime of electrons; (2) the band gap of

15   $SiW_{11}Ni/TiO_2$ turns narrow and the response in the visible region is expanded. The

16   good electrons transport makes it possible to increase the utilization percentage of

17   visible light.

18   Finally, a possible working mechanism of $SiW_{11}Ni/TiO_2$-P25 photoanode for

19   efficient DSSCs is proposed and shown in Scheme 1. Upon being excited by the

20   illumination, the sensitizer dye molecules (N719) absorb the visible light and reach

21   their excited state (Dye*), by which electrons are excited from the HOMO to the

22   LUMO of the dye and photoelectrons will be injected from the LUMO of the dye to

23   the conduction band (CB) of TiO_2. At the same time, $SiW_{11}Ni$ particles absorb the

24   visible light into HPB (heteropolyblue) and remove holes from photoanode and then

14

1   inject them into the electrolyte. Unfortunately, a certain amount of injected electrons

2   return back from the CB of TiO_2 to HOMO of the dye before flowing into the external

3   circuit and some occur at the $SiW_{11}Ni/TiO_2$-P25/dye/electrolyte interface (dotted lines

4   in Scheme 1).[46] Particularly at the interfacial region, electrons recombination may be

5   overcome by introducing a powerful electrons acceptor. HPA leads to a decrease in

6   the recombination of electrons-hole because it accepts electrons from the TiO_2

7   conduction band so that electrons and holes can be separated as effective charge

8   carriers. Thus, HPA can serve as an electrons mediator, which shuttles electrons from

9   the electrolyte to the electrode effectively and helps to enhance the efficiencies. Under

10 illumination, the most injected electrons are recaptured by I_3^- before being extracted

11 to the external circuit. $SiW_{11}Ni$ captured the returning electrons to reduce itself to

12 form HPB. In this process, HPB also plays an important role in the DSSCs, absorbing

13 visible light into HPB^*, and HPB^* can inject electrons into the CB of TiO_2.[47,48] The

14 intermediate HPB was excited and reduced to the excited $SiW_{11}Ni$, which

15 subsequently returned to the ground state of $SiW_{11}Ni$.[49] Thus, it avoided the

16 photoreduction of iodine on the surface of the photoanode. Such an effective electrons

17 transfer in $SiW_{11}Ni$ can remove the fast electrons–hole recombination on TiO_2 and is

18 ascertained from the lifetime of the transient species available in the literature.[49]

19 Meanwhile, the oxidized dye and $SiW_{11}Ni$ are regenerated by I^-. As a result, the

20 absorbed photon energy is converted to heat through the two coupled redox cycles

21 involving sensitized electrons injection, dye regeneration and electrons recapture by

22 I_3^-. In general, the introduction of $SiW_{11}Ni$ can inhibit most of the backward reactions

23 that take place in standard dye sensitized solar cell system and then increase the

24 photocurrent generation by enhancing the absorption and retarding the regeneration of

25 electrode. All the above merits improved the performance and stability of DSSCs.
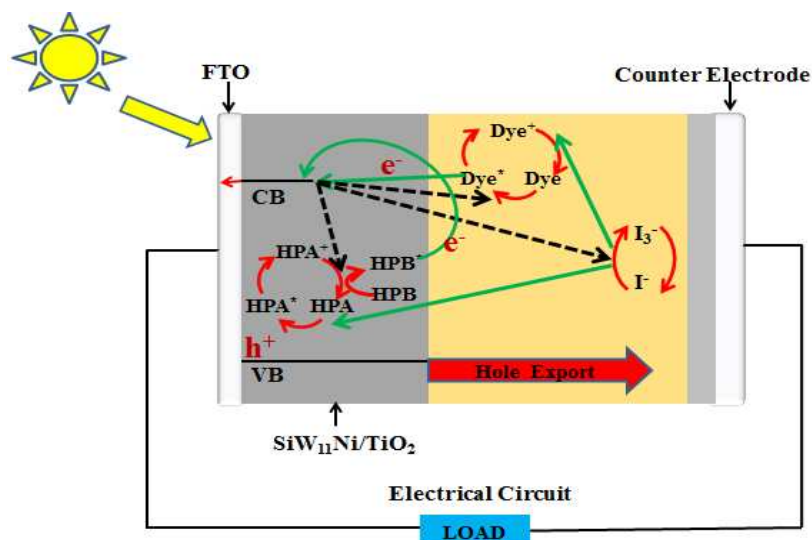
1
2   **Scheme 1** Mechanism of photoinduced electrons flow through HPA/TiO$_2$ film electrode.

3   ## Conclusions

4   In summary, we have successfully synthesized a novel composite material of

5   SiW$_{11}$Ni/TiO$_2$ that can effectively modify photoanode. The DSSC based on

6   SiW$_{11}$Ni/TiO$_2$-P25 (2:8) photoanode exhibits high performance in both J_{sc} and η,

7   increasing from 13.28 mA cm^{-2} and 6.42% (P25 as photoanode) to 17.38 mA cm^{-2} and

8   7.82% (SiW$_{11}$Ni/TiO$_2$-P25 as photoanode). The overall improvement in the

9   photocurrent and efficiency is 31% and 22% respectively. The considerable

10 improvement in the J_{sc} and η can be attributed to the following reasons by the

11 introduction of SiW$_{11}$Ni: (1) excellent electrons injection and good electrons transport;

12 (2) retarding the electrons recombination between the oxide electrolyte and dye

13 cations; (3) the narrowed band gap of SiW$_{11}$Ni/TiO$_2$ and the expanded response to the

14 visible region. All these merits are beneficial to the improvement of the performance

15 of the device.

16 ## Acknowledgements

Notes and references

1 B. O'Regan and M. Grätzel, *Nature*, 1991, **353**, 737−740.

2 M. K. Nazeeruddin, A. Kay, I. Rodicio, R. H. Baker, E. Müller, P. Liska, N. Vlachopoulos and M. Grätzel, *J. Am. Chem. Soc.*, 1993, **115**, 6382–6390.

3 Y. T. Shi, C. Zhu, L. Wang, C. Y. Zhao, W. Li, K. K. Fung, T. L. Ma, A. Hagfeldt and N. Wang, *Chem. Mater.*, 2013, **25**, 1000–1012.

4 G. Li, M. Liang, H. Wang, Z. Sun, L. N. Wang, Z. H. Wang and S. Xue, *Chem. Mater.*, 2013, **25**, 1713–1722.

5 S. Kuwahara, S. Taya, N. Osada, Q. Shen, T. Toyoda and K. Katayama, *Phys. Chem. Chem. Phys.*, 2014, **16**, 5242–5249.

6 P. T. Hsiao, Y. L. Tung and H. S. Teng, *J. Phys. Chem. C*, 2010, **114**, 6762–6769.

7 P. R. F. Barnes, A. Y. Anderson, J. R. Durrant and B. C. O'Regan, *Phys. Chem. Chem. Phys.*, 2011, **13**, 5798–5816.

8 B. C. O'Regan, K. Bakker, J. Kroeze, H. Smit, P. Sommeling and J. R. Durrant, *J. Phys. Chem. B*, 2006, **110**, 17155–17160.

9 J. Nissfolk, K. Fredin, A. Hagfeldt and G. Boschloo, *J. Phys. Chem. B*, 2006, **110**, 17715–17718.

10 Y. F. Zhang, H. R. Zhang, Y. F. Wang and W. F. Zhang, *J. Phys. Chem. C*, 2008, **112**, 8553–8557.

11 J. Li, W. Zhang, L. Zhang and Z. S. Wang, *Phys. Chem. Chem. Phys.*, 2014, **16**, 7334–7338.

12 S. H. Kang, H. S. Kim, J. Y. Kim and Y. E. Sung, *Mater. Chem. Phys.*, 2010, **124**, 422–4[26].

13 D. Mercier, S. Boujday, C. Annabi, R. Villanneau, C. M. Pradier and A. Proust, *J. Phys. Chem. C*, 2012, **116**, 13217−13224.

14 F. M. Toma, A. Sartorel, M. Iurlo, M. Carraro, P. Parisse, C. Maccato, S. Rapino, B. R. Gonzalez, H. Amenitsch, T. Da Ros, L. Casalis, A. Goldoni, M. Marcaccio,

G. Scorrano, G. Scoles, F. Paolucci, M. Prato and M. Bonchio, *Nat. Chem.*, 2010, **2**, 826−831.

15 Y. Shen, J. Peng, H. Q. Zhang, X. Yu and A. M. Bond, *Inorg. Chem.*, 2012, **51**, 5146−5151.

16 Z. X. Sun, F. Y. Li, L. Xu, S. P. Liu, M. L. Zhao and B. B. Xu, *J. Phys. Chem. C*, 2012, **116**, 6420−6426.

17 C. Zou, Z. J. Zhang, X. Xu, Q. H. Gong, J. Li and C. D. Wu, *J. Am. Chem. Soc.*, 2012, **134**, 87−90.

18 Y. Ding, W. Zhao, W. F. Song, Z. X. Zhang and B. C. Ma, *Green Chem.*, 2011, **13**, 1486−1489.

19 S. Landsmann, M. Wessig, M. Schmid, H. Colfen and S. Polarz, *Angew. Chem. Int. Ed.*, 2012, **51**, 5995−5999.

20 S. M. Wang, L. Liu, W. L. Chen, Z. M. Su, E. B. Wang and C. Li, *Ind. Eng. Chem. Res.*, 2014, **53**, 150–156.

21 L. H. Wang, L. Xu, Z. C. Mu, C. G. Wang and Z. X. Sun, *J. Mater. Chem.*, 2012, **22**, 23627–23632.

22 A. Tézé and G. Hervé, *J. Inorg. Nucl. Chem.*, 1977, **39**, 999–1002.

23 R. H. Ma and F. P. Wang, *Chin. J. Inorg. Chem.*, 2007, **23**, 445–450.

24 G. Peng, C. W. Hu, L. D. Chen and E. B. Wang, *Function Materials.*, 2001, **10**, 1122–1130.

25 J. B. Yin and X. P. Zhao, *J. Phys. Chem. B*, 2006, **110**, 12916–12925.

26 J. J. Lin, Y. U. Heo, A. Nattestad, Y. Yamauchi, S. X. Dou and J. H. Kim, *Electrochim. Acta*, 2015, **153**, 393–398.

27 J. J. Lin, L. Zhao, Y. U. Heo, L. Z. Wang, F. H. Bijarbooneh, A. J. Mozer, A. Nattestad, Y. Yamauchi, S. X. Dou and J. H. Kim, *Nano Energy*, 2015, **11**, 557–567.

28 J. J. Lin, A. Nattestad, H. Yu. Y. Bai, L. Z. Wang, S. X. Dou and J. H. Kim, *J. Mater. Chem. A*, 2014, **2**, 8902–8909.

29 W. Q. Wu, H. S. Rao, H. L. Feng, H. Y. Chen, D. B. Kuang and C. Y. Su, *Nano Energy*, 2014, **9**, 15–24.

30   G. Jeong, J. G. Kim, M. S. Park, M. Seo, S. M. Hwang, Y. U. Kim, Y. J. Kim, J. H. Kim and S. X. Dou, *ACS Nano*, 2014, **8**, 2977–2985.

31   G. Rothenberger, D. Fitzmaurice and M. Grätzel, *J. Phys. Chem.*, 1992, **96**, 5983–5986.

32   G. Boschloo and A. Hagfeldt, *Acc. Chem. Res.*, 2009, **42**, 1819–1826.

33   D. Cahen and G. Hodes, *J. Phys. Chem. B*, 2000, **104**, 2053–2059.

34   S. R. Raga, E. M. Barea and F. F. Santiago, *J. Phys. Chem. Lett.*, 2012, **3**, 1629–1634.

35   G. L. Shang, J. H. Wu, S. Tang, L. Liu and X. P. Zhang, *J. Phys. Chem. C*, 2013, **117**, 4345−4350.

36   J. X. Zhao, X. H. Lu, Y. Z. Zheng, S. Q. Bi, X. Tao, J. F. Chen and W. L. Zhou, *Electrochem. Commun.*, 2013, **32**, 14–17.

37   J. Liu, H. T. Yang, W. W. Tan, X. W. Zhou and Y. Lin, *Electrochim. Acta*, 2010, **56**, 396–400.

38   W. Q. Liu, D. X. Kou, M. L. Cai, L. H. Hu, J. Sheng, H. J. Tian, N. Q. Jiang and S. Y. Dai, *J. Phys. Chem. C*, 2010, **114**, 9965–9969.

39   G. Schlichthörl, S. Y. Huang, J. Sprague and A. J. Frank, *J. Phys. Chem. B*, 1997, **101**, 8141–8155.

40   Y. P. Fu, M. Peng, Z. B. Lv, X. Cai, S. C. Hou, H. W. Wu, X. Yu, H. Kafafy and D. C. Zou, *Nano Energy*, 2013, **2**, 537–544.

41   F. Gu, W. J. Huang, S. F. Wang, X. Cheng, Y. J. Hu and P. S. Lee, *Phys. Chem. Chem. Phys.*, 2014, **16**, 25679–25683.

42   K. Zhu, N. R. Neale, A. Miedaner and A. J. Frank, *Nano Lett.*, 2007, **7**, 69–74.

43   K. Zhu, T. B. Vinzant, N. R. Neale and A. J. Frank, *Nano Lett.*, 2007, **7**, 3739–3746.

44   J. Bisquert, A. Zaban, M. Greenshtein and I. Mora-Seró, *J. Am. Chem. Soc.*, 2004, **126**, 13550–13559.

45   A. Zaban, M. Greenshtein and J. Bisquert, *ChemPhysChem*, 2003, **4**, 859–864.

46   M. Wielopolski, K. E. Linton, M. Marszalek, M. Gulcur, M. R. Bryce and J. E. Moser, *Phys. Chem. Chem. Phys.*, 2014, **16**, 2090–2099.

1   47   Ning. Fu and G. X. Lu, *Appl. Surf. Sci.*, 2009, **255**, 4378–4383.

2   48   S. K. Parayil, Y. M. Lee and M. Yoon, *Electrochem. Commun.*, 2009, **11**,

3   1211–1216.

4   49   M. Yoon, J. A. Chang, Y. Kim, J. R. Choi, K. Kim and S. J. Lee, *J. Phys. Chem. B*,

5   2001, **105**, 2539–2545.